Dynamic Organization of Myristoylated Src in the Live Cell Plasma Membrane

Adam W. Smith,[†‡§] Hector H. Huang,[†¶] Nicholas F. Endres,[¶] Christopher Rhodes,[†‡] and Jay T. Groves[†‡*]*

[†]Howard Hughes Medical Institute, Department of Chemistry, University of California, Berkeley, California 94720, United States

[‡]Physical Biosciences and Materials Sciences Divisions, Lawrence Berkeley National Laboratory, Berkeley, CA 94720, United States

[¶]Howard Hughes Medical Institute, Department of Molecular and Cell Biology, University of California, Berkeley, California 94720, United States

[§]Department of Chemistry, University of Akron, Akron OH 44303.

AUTHOR INFORMATION

Corresponding Authors

*jtgroves@lbl.gov, *asmith5@uakron.edu

ABSTRACT

The spatial organization of lipid-anchored proteins in the plasma membrane directly influences cell signaling, but measuring such organization *in situ* is experimentally challenging. The canonical oncogene, c-Src, is a lipid anchored protein that plays a key role in integrin-mediated signal transduction within focal adhesions and cell-cell junctions. Because of its activity in specific plasma membrane regions, structural motifs within the protein have been hypothesized to play an important role in its sub-cellular localization. This study used a combination of time-resolved fluorescence fluctuation spectroscopy and super-resolution microscopy to quantify the dynamic organization of c-Src in live cell membranes. Pulsed-interleaved excitation fluorescence cross-correlation spectroscopy (PIE-FCCS) showed that a small fraction of c-Src transiently sorts into membrane clusters that are several times larger than the monomers. Photoactivated Localization Microscopy (PALM) confirmed that c-Src partitions into clusters with low probability and showed that the characteristic size of the clusters is 10-80 nm. Finally, time-resolved fluorescence anisotropy measurements were used to quantify the rotational mobility of c-Src to determine how it interacts with its local environment. Taken together, these results build a quantitative description of the mobility and clustering behavior of the c-Src non-receptor tyrosine kinase in the live cell plasma membrane.

KEYWORDS Fluorescence correlation spectroscopy, Photoactivated localization microscopy, lipid anchored proteins, membrane protein structure and dynamics.

INTRODUCTION

Lipid modifications target proteins to the plasma membrane and play a key role in signal transduction.[1, 2] Among these lipid modifications is N-terminal myristoylation, which is found on up to 3% of the human proteome.[3, 4] The myristoyl group is a 14 carbon acyl chain enzymatically attached to N-terminal glycine by the enzyme N-myristoyl transferase. For singly myristoylated proteins, stable membrane binding requires insertion of the myristoyl group into the hydrophobic region of the lipid bilayer as well as a secondary stabilizer like favorable electrostatic interactions between protein side chains and charged lipids.[3, 5] While it is well-established that both of these structural motifs are necessary for membrane localization and function, it is unclear to what degree a single myristoylation anchor drives organization within the plasma membrane.[4] In this paper we investigated the clustering behavior of a model myristoyl anchored protein, c-Src, in live cells with several advanced optical microscopy and spectroscopy techniques. We found that c-Src is primarily monomeric in the plasma membrane, but that it interacts weakly with large membrane clusters.

The c-Src protein plays a key role in integrin-mediated signal transduction within focal adhesions and cell-cell junctions. Because of its activity in well-defined plasma membrane regions, it is hypothesized that structural motifs within the protein play an important role in sub-cellular localization.[6] In this study our aims were to quantify the clustering potential of full length c-Src live cells and isolate the contribution of the lipid anchor motif of c-Src. To this end we used a truncated c-Src chimera, Src_{16}, which included a fluorescent protein fused to the 16 N-

terminal amino acids and a six residue linker region. This approach has been used for a number of different lipid-anchored proteins,[7-13] but there are relatively few studies of the Src anchor specifically.[14-17] We characterized the clustering and mobility of Src_{16} in the live cell plasma membrane using a suite of modern tools in fluorescence spectroscopy and microscopy. First, we used pulsed interleaved excitation (PIE) and time-correlated single photon counting (TCSPC) to measure fluorescence correlation (FCS) and cross-correlation (FCCS) spectra of Src_{16}-mCherry and Src_{16}-eGFP in live Cos-7 cells. To determine if the clustering behavior of the anchor construct is conserved in the full-length protein, we compared the FCS and FCCS measurements of a similarly truncated isoform of Src derived from mouse ($mSrc_{16}$) with the full-length form ($mSrc_{FL}$). Measurements were also made in Jurkat T-cells to compare the clustering behavior of these constructs in the plasma membrane of an alternate cell line. Time-resolved fluorescence anisotropy measurements revealed the rotational mobility of the fluorophores, allowing further characterization of Src mobility at the membrane. In addition to the time-resolved methods above, we also measured Src clustering with Photoactivated Localization Microscopy (PALM) which can resolve cluster sizes down to 10's of nanometers.

Our results show that the Src_{16} membrane anchor transiently associates with plasma membrane clusters. The correlation spectroscopy shows that the majority of anchors are highly mobile, with an effective diffusion coefficient ($D = 0.95 \pm 0.30\ \mu m^2 s^{-1}$ in the Cos-7 plasma membrane and $D = 1.36 \pm 0.48\ \mu m^2 s^{-1}$ in the Jurkat plasma membrane) comparable to that reported for lipids in the plasma membrane.[18-20] PIE-FCCS data show that the cross-correlation is density dependent, consistent with a model in which a subset of the Src_{16} anchor in the plasma membrane is bound to large clusters. From the time decay of the cross-correlation function, we conclude that these are mobile clusters significantly larger than the monomers. From the PALM images we see that

the Src_{16} anchor clusters into 10-80 nm features with a relatively low probability, consistent with the PIE-FCCS data. All of these observations contribute to a sophisticated description of the mobility and clustering behavior of the lipid anchor motif of the Src protein, one where the vast majority of Src is highly mobile, while the small remaining fraction is associated with large (10-80 nm) membrane clusters.

EXPERIMENTAL

Protein Constructs

The Src-derived chimeras used for this study included C-terminal mCherry or eGFP fusions to the following proteins:

1. **Src_{16}** (N-terminal residues 1-16 of human c-Src)
2. **Src_{16}-ICM** (same as above with kinase domain of EGFR)
3. **Src_{13}-GCN4-ICM** (N-terminal residues 1-13 of human c-Src, the GCN4 peptide, and the kinase domain of EGFR)
4. **$mSrc_{16}$** (N-terminal residues 1-16 or mouse c-Src)
5. **$mSrc_{FL}$** (Full-length (FL) mouse c-Src)

Constructs were cloned into the mammalian expression vector pEGFP (Clonetech) as previously reported.[21] The Src_{16}-eGFP or Src_{16}-mCherry constructs were generated by insertion of the c-Src plasma membrane localization sequence (MGSSKSKPKDPSQRRR) N-terminal to eGFP or mCherry with a six amino acid spacer (GGGGLK) in between. Src_{16}-ICM constructs included the c-Src plasma membrane localization sequence inserted N-terminal to the epidermal growth factor receptor (EGFR) intracellular module (ICM, residues 645-1186) with a four amino acid spacer in between. Src_{13}-GCN4-ICM included the GCN4 coiled-coil sequence

(VKQLEDKVEELLSKNAHLENEVARLKKLV) in between the c-Src localization sequence and the intracellular module. The localization sequence used for Src_{13}-GCN4-ICM lacked the last three arginines of the c-Src motifs as reported previously.[21] In Jurkat cell experiments, the $mSrc_{16}$-eGFP, $mSrc_{16}$-mCherry, $mSrc_{FL}$-eGFP, or $mSrc_{FL}$-mCherry constructs were derived from the murine isoform of c-Src (Addgene plasmid 13663: pCMV5 mouse src). The $mSrc_{16}$-eGFP and $mSrc_{16}$-mCherry also fuse the 16 amino acid N-terminal localization sequence of mouse c-Src (MGSNKSKPKDASQRRR) to an eGFP or a mCherry protein with a six amino acid spacer (GGGGLE) in between. $mSrc_{FL}$-eGFP and $mSrc_{FL}$-mCherry similarly fuses the entire Src gene to the N-termini of eGFP or mCherry with the same six amino acid linker in between. The sequence of the gene can be found in the NCBI database (Gene ID: 20779).

Cell Culture

Cos-7 cells were cultured in Dulbecco's Modified Eagle's Medium supplemented with 10% fetal bovine serum (FBS) and streptomycin/penicillin. Cells were transiently transfected with Fugene 6 (Roche) and cultured for 24 hr after transfection, followed by 12 hr serum starvation. Cells were grown on glass coverslips etched with a 2:1 mixture of nitric and hydrochloric acids. Fluorescence measurements were done in a phenol-red free Dulbecco's Modified Eagle's Medium.

Jurkat cells were cultured in RPMI 1640 supplemented with 10% fetal bovine serum (FBS), 1% Sodium-pyruvate, and streptomycin/penicillin. Cells were transiently transfected with Lipofectamine 2000 (Invitrogen) and cultured for 16-20 hr before being deposited on poly-L-lysine coated coverslips as described previously.[11]

Instrument details for PIE-FCCS

Two microscopes were used for PIE-FCCS measurements, each described in previous publications.[11, 21] For Src_{16} and Src_{13} measurements (Figures 1-4) Two lasers were used to excite eGFP and mCherry fluorophores, a 100 ps, pulsed 482 nm diode laser and a 250 fs pulsed 561 nm laser, both operating at 10 MHz repetition rate. The powers were set to approximately 1 μW, measured before entering the microscope. A multi-line dichroic (z405/488/561rpc, Chroma Technology Corp.) directed the light into the objective (CFI APO 100X Oil TIRF NA 1.49, Nikon Instruments Inc.), and the emitted fluorescence was filtered (z405/488/561m, Chroma Technology Corp.) and directed to a long wave pass dichroic beamsplitter (FF562-Di02-25x36, Semrock Inc.), which split the light to the single photon avalanche diodes. The passed light was filtered with a 612/69 bandpass filter (FF01-612/69-25, Semrock Inc.), while the reflected light was filtered with a 520/25 bandpass filter (FF01-520/35-25, Semrock Inc.). Detector output was recorded with a time-correlated single photon counting module (PicoHarp 300, PicoQuant Photonics Inc.) with the time resolution set to 32 ps. The PIE-FCCS data for $mSrc_{16}$ and $mSrc_{FL}$ (Figure 6) was collected identically to that described in an earlier study.[11]

Data collection procedure

PIE-FCCS data was collected in live cells expressing both eGFP and mCherry chimeras co-transfected about 24 hour before the experiment. During data collection, the temperature of the cells was maintained with a water-bath stabilized heating stage at slightly below room temperature (20 °C) or at physiological temperature (37 °C) as indicated in figure captions. Cells were chosen based on their relatively similar expression of eGFP and mCherry. Cos-7 cells have a fried egg morphology, and at the edges, the cell thickness is less than a few hundred nanometers. All the FCCS measurements were made near the cell periphery, meaning that we were measuring the apical and basal membrane simultaneously, with very little cytoplasm (see

Endres et. al. (ref [21]) for detailed discussion). In choosing spots for laser excitation, we explicitly avoided large (>1 μm), immobile, high intensity features. We restricted our analysis to cell densities ranging from 100-2000 molecules per μm^2. For each cell, five 15 s measurements were made in succession and analyzed as described below.

Data analysis

The time tagged data files from each color channel were processed by binning the gated, time-tagged data into a time-dependent intensity I(t). The bin time was set to 10 μs. A time gate was applied to only count photons detected by the 520 nm (or 612 nm) filtered detector that arrived between 1 ns before and 40 ns after the 482 nm (or 561 nm) laser pulse. The time-dependent intensity was used to calculate the correlation function:

$$G_i(\tau) = \frac{\langle \delta I_i(t) \cdot \delta I_i(t+\tau) \rangle}{\langle I_i(t) \rangle^2} \quad (1)$$

Where the subscript, i, indicates either the red (R) or green (G) color channel and

$$\delta I_i(t) = I_i(t) - \langle I_i(t) \rangle \quad (2)$$

The cross-correlation function was calculated according to the following equation:

$$G_X(\tau) = \frac{\langle \delta I_R(t) \cdot \delta I_G(t+\tau) \rangle}{\langle I_R(t) \rangle \cdot \langle I_G(t) \rangle} \quad (3)$$

The subscripts G and R indicate the intensity of the 520 and 612 nm filtered detectors, respectively. All three correlation functions (G_R, G_G, and G_X) are fit to the following equation from from 10^0 to 10^4 ms:

$$G_i(\tau) = \frac{1}{\langle N_i \rangle} \cdot \frac{1}{1 + {}^{\tau}/_{\tau_{Di}}} \quad (4)$$

where $\langle N_i \rangle$ is the average number of molecules and τ_D is the characteristic dwell time of the molecules in the observation area. Only single component diffusion was observed in our

experiments, consistent with diffusion in a 2D membrane environment. We did not include an additional term to account for triplet state relaxation because it was more than an order of magnitude faster than the dwell time, τ_D.

Fitting the data to Eq. 4 allowed us to quantify the average number of diffusing species, in the laser spot (N_R, N_G and N_X, respectively) from early time amplitudes of the correlation functions. We then calculated a relative correlation value, F_x, which represents the extent to which the diffusion of GFP and mCherry-labeled molecules are correlated:

$$F_X = \frac{G_X(0)}{max\left(G_R(0), G_G(0)\right)} \tag{5}$$

The PIE-FCCS measurements of $mSrc_{16}$ and $mSrc_{FL}$ in Jurkat cells (Fig. 6) were scaled by a routine described in a previous publication.[11] F_x values from $mSrc_{16}$ and $mSrc_{FL}$ measurements were scaled relative to *in vitro* standards. Samples of eGFP and mCherry tethered to a Ni-DOGS containing supported lipid bilayer via 12x histidine tag represent uncorrelated diffusion, while a fusion of eGFP-mCherry connected by a small peptide linker bilayer served as a control for correlated diffusion. Due to the dead time of the TCSPC acquisition, F_x values of the *in vitro* samples decrease with respect to measured intensity, which were fit to a linear regression. F_x values were then rescaled according to measured intensity, such that the relative scaled correlation of the fully correlated diffusion of the eGFP-mCherry fusion protein was 1 and that of the uncorrelated diffusion of the eGFP and mCherry was 0.

Photoactivated localization microscopy

For PALM imaging, the Src_{16} construct described above was fused to the N-terminus of photoswitchable cyan fluorescent protein, PS-CFP2 (Evrogen Joint Stock Company, Moscow, Russia) instead of eGFP or mCherry. Cos-7 cells were cultured and transfected as above and imaged live. Live cells were imaged on an inverted microscope (Nikon Eclipse Ti; Technical

Instruments, Burlingame, CA, USA) using the same objective as in the PIE-FCCS measurements. TIRF microscopy was performed using a fiber-coupled Nikon TIRF illuminator and a custom-built laser source.[22] A 405 nm laser (Cube 405-100; Coherent Inc, Santa Clara, CA) was used to photoactivate PS-CFP2. A 488 nm laser (Sapphire HP; Coherent Inc., Santa Clara, CA) was used to image the photo-activated Src_{16}-PS-CFP2 fusion proteins at excitation power densities of 10 $kW \cdot cm^{-2}$. Images were acquired with an EM-CCD camera (iXon 597DU; Andor Inc, South Windsor, CT) operated at full EM gain. The power of the 405 nm photoactivation laser was continually adjusted throughout the experiment to optimize the number of bright molecules. Approximately 10,000 to 15,000 images (~10 Hz frame rate) were collected for each cell. Single molecule localization was done using a MatLab script provided by Sam Hess following a previously published protocol.[23] The image series was background corrected using the summed wide field method.[24] Single molecules in each frame were identified and localized via two-dimensional Gaussian centroid analysis, and the set of positions were used to construct the final image. The error in the location for each particle was used to quantify the localization precision. A histogram of those errors is called the localization precision histogram, the mean value of which is 22 nm for the data shown in Fig. 5A and 5B.

Even at high laser excitation intensities, there is still some probability of localizing a molecule in several successive frames before it is photobleached. This would lead to overcounting single molecules in the final image. To remove this artifact we used the frame sequence information along with the fit positions in a particle tracking analysis. The tracks were allowed to have up to one empty frame to avoid artifacts from thresholding and allowed to drift up to 300 nm, which matches the mean squared displacement for 10 Hz frame rate at the diffusion rate measured using FCS. For each track only the first position was used to calculate the pair correlation

function. The pair correlation function was calculated using rectangular boundary conditions to avoid cell boundary edge effects.[25]

$$g(r) = \frac{\eta(r)X^2Y^2}{N(N-1)\cdot\delta r\cdot[\pi XYr - 2(X+Y)r^2 + r^3]} \quad (6)$$

Here, X and Y are the boundaries of a rectangular area within the cell. N is the total number of particles. $\eta(r)$ is the number of particle pairs with separation distance $r \pm \delta r/2$. $g(r)$ was calculated for several cells, a representative example of which is plotted in Fig. 5C.

Time resolved fluorescence anisotropy methods

Time-tagged, time-resolved photon streams were collected using the same confocal optical system described above. Samples were excited by second harmonic generation of a Ti:sapphire pulsed laser (80 MHz pulse rate) tuned to 970 nm (Spectra Physics, Santa Clara, CA). This produced a 485 nm pulse train, which was directed through a linear polarizer. Emission was divided between two SPADs using a polarizing beamsplitter cube, and sampled at 4 ps resolution using a PicoHarp 300 card (PicoQuant, Berlin, Germany). Time-resolved anisotropy decays were fit in MATLAB from the two photodiode signals $I_{\parallel}$ and $I_{\perp}$ using nonlinear least squares to minimize residuals according to:

$$\chi^2 = \sum_i^n w_i \left[\frac{I_{\parallel,i} - GI_{\perp,i}}{I_{\parallel,i} + GI_{\perp,i}} - r_0 e^{-\frac{t_i}{\theta}}\right] \quad (7)$$

for TCSPC channel i of n, and fitting for rotational correlation time θ and detector response ratio G. Residual weighting factor w_i was computed from standard error propagation of two Poisson processes, and r_0 determined by a prior comparison of membrane-bound Src-GFP with fluorescein isothiocyanate. Instrument response functions decayed much faster (250 ps) than the timescale of fluorophore anisotropy decay (50-150 ns), and hence were not reconvolved during fitting.

RESULTS AND DISCUSSION

Src anchor cross-correlation is density dependent

PIE-FCCS measurements were first carried out on the Src_{16} constructs in live Cos-7 cells at 20 °C. Single cells were interrogated with the 482 nm and 561 nm lasers simultaneously (Fig 1A), and the fluorescence signal was collected, time-gated (Fig 1B), and processed as described in the Experimental section. Sample data from individual cells is shown in Fig. 1C and 1D. The FCS data (red and green curves in Fig 1C and 1D) were used to calculate the density and mobility of the proteins, and the FCCS data (blue curves in Fig. 1C and 1D) were used to calculate the relative correlation, F_x. which can vary from 0 to 1, with 1 being the theoretical maximum. The actual maximum for our positive control construct was closer to 0.2 as explained below. By comparing Fig. 1C and 1D, it is clear that for different cells the relative amplitude of the cross-correlation spectrum can be substantially different.

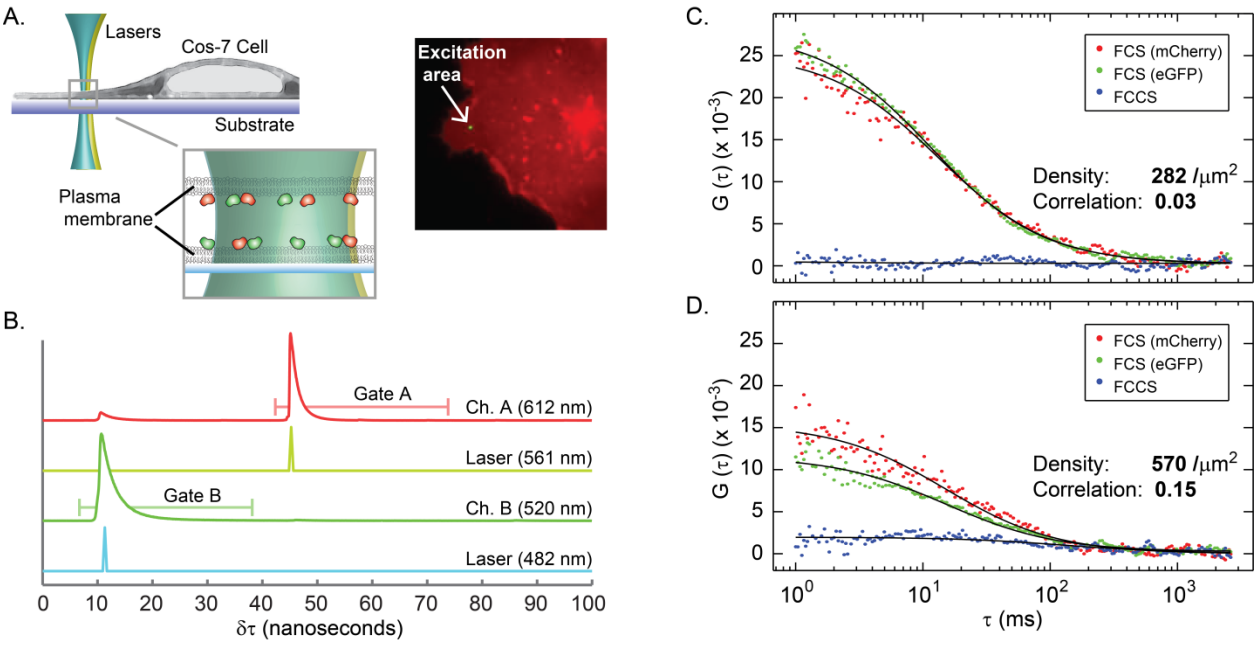

Figure 1 – Overview of PIE-FCCS experiments (A) For live cell measurements, the 482 and 561 nm lasers are focused to a diffraction limited spot (~500 nm diameter) near the edge of the cell to avoid large, bright clusters of fluorescence. Fluorescence is detected from the upper and lower membranes simultaneously due to the width of the plasma membrane (~200 nm) relative to the z-resolution of the confocal detection (~1 μm). On the right, an epi-fluorescence micrograph of Src_{16}-mCherry in a Cos-7 cell is overlaid with an image of the laser-excited fluorescence in the same cell. (B) A pulse timing diagram shows the arrival time of the two laser pulses and the lifetime histogram for each detection channel. (C & D) Fluorescence correlation spectroscopy of Src_{16}-eGFP, Src_{16}-mCherry anchors coexpressed in Cos-7 cells at 20 °C. Panel (C) shows a representative set of FCS data for a cell expressing the indicated *low* density of membrane anchors. Autocorrelation spectra of Src_{16}-eGFP and Src_{16}-mCherry are shown in green and red respectively, and the cross-correlation spectrum is shown in blue. Fits to the data using a 2D diffusion model are shown in black, and the relative correlation for this data set is indicated in the bottom right corner of the graph. Panel (D) shows the same data set acquired for cells expressing the indicated *high* density of anchors. The cross-correlation curve in this case clearly displays a non-zero amplitude at early times indicating correlated diffusion of the two anchor populations.

To determine if the relative correlation, F_x, is dependent on the protein density, we plot F_x versus the Src_{16} density in Fig. 2A. The surface density was calculated by summing the average number of particles from the FCS curve fitting ($N_g + N_r$), and dividing by the calibrated detection area (radius ω_{xy} = 205 nm, area = 0.132 μm^2). The Src_{16} data show a clear trend of increasing correlation at higher molecular densities. In order to calibrate the expected maximum correlation

for our instrument, we also measured the PIE-FCCS data for Cos-7 cells expressing eGFP and mCherry labeled Src_{13}-GCN4-ICM, which is known to dimerize.[21, 26] The Src_{13}-GCN4-ICM data show no clear trend with density (Fig. 2B) and have an average $F_x = 0.18 \pm 0.07$ as mentioned above. This is approximately half the value reported for an eGFP-mCherry fusion construct,[27] and it reflects the probability of forming mCherry-mCherry dimers and eGFP-eGFP dimers relative to mCherry-eGFP dimers.

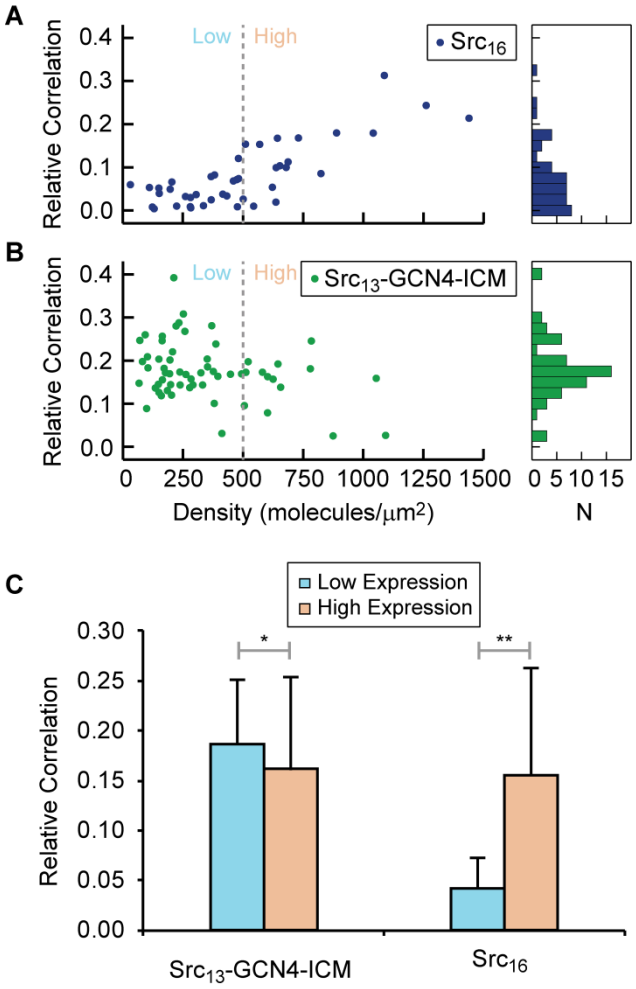

Figure 2 – The relative correlation of Src_{16} is density dependent at 20 °C. **(A)** The scatter plot shows the relative correlation, F_x, for the Src_{16} anchor as function of anchor density for 43 cells. The graph on the right is a histogram (0.025 bin size) of the data in the right plot. Both graphs

share the same y-axis. **(B)** This scatter plot shows the relative correlation of the dimerized Src_{13}-GCN4-ICM anchor as a function of density for 61 cells. As above, the graph on the right is a histogram of the Src_{13}-GCN4-ICM anchor with the same bin size and x-axis as in (A). **(C)** Bar chart shows the average and standard deviation of the relative correlation at all densities (green) for each anchor type and at two density ranges (blue: low < 500 molecules/μm^2, red: high > 500 molecules/μm^2). (*p = 0.35, **p <<0.001, calculated using a two-sample Student's t-test, with two tails and unequal variances)

The difference between the high and low expression levels is shown in Fig. 2C, which compares the average relative correlation, F_x, at high (>500 molecules/μm^2) and low (<500 molecules/μm^2) densities. As can be seen, the average cross correlation for Src_{16} is 0.04 ± 0.03 at low densities and jumps to 0.16 ± 0.11 at high densities, which is near the value measured for the Src_{13}-GCN4-ICM dimer construct at high and low densities. Density dependent cross-correlation has been observed for other membrane anchors by our lab using similar techniques.[11] In that previous work the dependence was explained by partitioning of the anchors into pre-existing membrane clusters, so that the cross correlation grows as the clusters reach a labeling density that allows for two anchors of different color (eGFP or mCherry) in the same cluster. Here we also assign the observed density dependence to the partitioning probability rather than density activated clustering.

Src anchor partitioning is temperature dependent

In order to determine if the partitioning of Src_{16} anchors is similar at physiological temperature, we repeated the measurements in a stage heater maintained at 37 °C. As can be seen in Fig. 3, the trend of the relative correlation versus density changed substantially with temperature. The high

density region in particular is much more heterogeneous, with a stronger probability of observing no cross correlation. In the bar graph, it is clear that the average cross-correlation over the entire density range drops substantially from 20 °C to 37 °C, but that the relative difference between the high and low expression densities is maintained at 37 °C. The clearest feature common to both temperatures is that at molecular densities below 500 molecules/μm^2, the fraction correlated is low (0.04 ± 0.03 @ 20 °C and 0.02 ± 0.02 @ 37 °C).

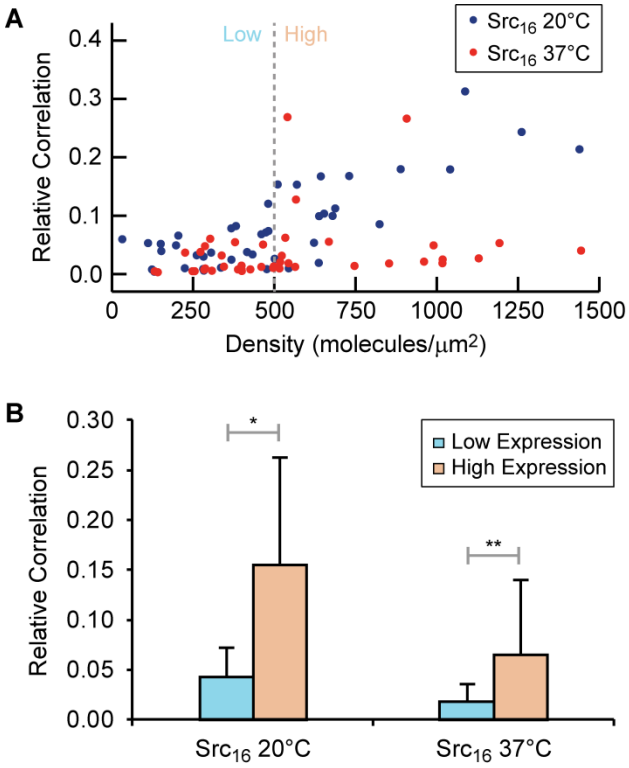

Figure 3 – At physiological temperature, partitioning into clusters is reduced. **(A)** Overlay of relative correlation versus density for Src_{16} at 20 °C (identical to Fig. 1A) and at 37 °C (for 45 cells). **(B)** Bar chart showing the average and standard deviation of the relative correlation for Src_{16} at 20 °C and 37 °C. High and low density ranges are the same as Fig. 1 (low < 500 molecules/μm^2, high > 500 molecules/μm^2). (*p << 0.001, **p = 0.0095)

Mobility of membrane bound Src anchors

FCS data (ie. Fig. 1C and 1D) have characteristic time decays, τ_D, which are related to the average dwell time of the molecule in the laser focus. This parameter can be used along with the calibrated radius of the observation area (ω_{xy} = 205 nm) to give an effective diffusion coefficient according to the following equation:

$$D_{eff} = \frac{\omega_{xy}^2}{4\tau_D} \tag{8}$$

The diffusion coefficient of several membrane anchored proteins measured by the eGFP FCS data is plotted in Fig. 4A. For comparison between the protein constructs, we show data collected at 37 °C. Under these conditions, the Src_{16} anchor has a diffusion coefficient, D_{eff} = 0.95 ± 0.30 $\mu m^2 s^{-1}$. This is comparable to the diffusion coefficient of a highly charged lipid, PIP_2, in the inner leaflet of the plasma membrane, and is 1.5-2 times lower than a singly charged lipid as measured by FCS.[28] It is substantially lower than the diffusion coefficient of cytosolic proteins, which can range from 10-70 $\mu m^2 s^{-1}$.[29-32] These comparisons are consistent with our conclusions that the PIE-FCCS measurements are dominated by membrane bound Src anchors and that the majority of Src anchors are free to diffuse as monomers.

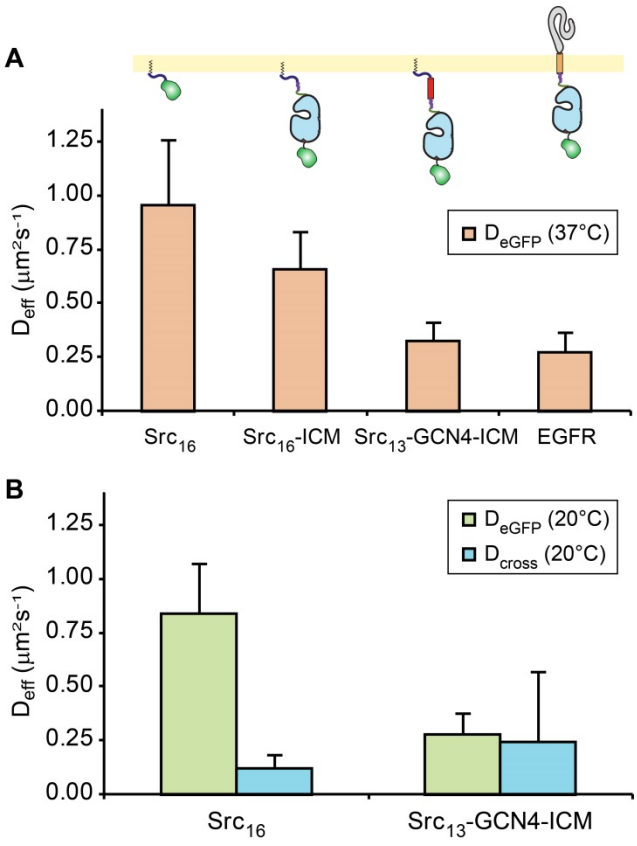

Figure 4 – Mobility of protein anchors. The FCS curves were fit to determine their characteristic decay times, τ_D, which was converted into a diffusion coefficient as described in the text. Plot **(A)** compares the diffusion coefficient D_{eGFP} measured from the FCS data of four eGFP-tagged membrane anchored proteins at 37 °C. Plot **(B)** compares the diffusion coefficient extracted from the FCS curves, D_{eGFP}, to the diffusion coefficient extracted from the FCCS curves, D_{cross}, for Src_{16} and Src_{13}-GCN4-ICM at 20 °C. From this comparison we conclude that the subset of Src_{16} anchors giving rise to cross correlation have a 10-fold slower D_{eff} than the majority of anchors that give the D_{eff} extracted from the FCS curves. For A and B, the height of the columns is the mean value for multiple cells and the error bars represent the standard deviation.

When the large kinase domain from the EGFR protein is fused to the Src_{16} anchor the diffusion coefficient drops to $0.66 \pm 0.17\ \mu m^2 s^{-1}$ (Fig. 4). While there is some controversy in understanding the scaling laws for protein diffusion in cell membranes, the proposals range from $1/\ln(R)$ according to the Saffman Delbruck model[33] and 1/R according to some recent reports.[34, 35] For simplicity, if we assume 1/R scaling, comparing Src_{16} to Src_{16}-ICM would correspond to a 1.45 factor increase in the radius. Because both proteins share the same lipid anchor and have the same clustering potential,[21] this means that the interaction of the kinase domain either with the membrane or other membrane associated proteins leads to an increase in the effective radius. For the GCN4-induced dimer, Src_{13}-GCN4-ICM, the diffusion coefficient is $0.32 \pm 0.09\ \mu m^2 s^{-1}$, which compared to the Src_{16}-ICM protein is a 2x increase in the radius under the assumed scaling rule. This is consistent with dimerization increasing the effective radius of the complex, and supports the conclusion that Src anchored proteins preferentially diffuse as monomers. For a full length transmembrane protein, EGFR, the diffusion coefficient is $0.27 \pm 0.09\ \mu m^2 s^{-1}$. In previous work, EGFR was shown to be monomeric in the plasma membrane,[21] so this decrease in the diffusion coefficient means that the effective radius has increased relative to the Src_{16}-ICM construct. This could result from several mechanisms, including protein-protein interactions, protein-lipid interactions, or compartmentalized diffusion. The mechanistic details of this observed trend are still under investigation.[36-38]

Clustered Src is less mobile than monomeric Src

We can also compare the diffusion coefficient obtained from the FCS curve, $G_g(\tau)$, with that of the FCCS curve, $G_x(\tau)$. For Src_{13}-GCN4-ICM, this comparison shows that the FCS and FCCS curves have the same time decay and consequently produce the same diffusion coefficient. This result supports the conclusion that Src_{13}-GCN4-ICM proteins are located in a homogeneous

population of diffusing species (i.e. dimers) that contribute equally to the FCS and FCCS curves. For the Src_{16} anchor, the FCS curves have a time decay that yields a diffusion coefficient of 0.84 ± 0.23 $\mu m^2 s^{-1}$ at 20 °C. In contrast, the time decay of the cross-correlation curves is significantly longer, yielding a diffusion coefficient of 0.12 ± 0.07 $\mu m^2 s^{-1}$ for cells with a relative correlation, $F_x > 0.075$. The discrepancy between the FCS and FCCS time decays suggests that Src anchor is only partially localized to the slow-moving clusters. The FCS data is dominated by species that display a diffusion coefficient near that of lipids in cell membranes. Combined with the lack of significant cross-correlation, this suggests that the dominant species is a monomer. The FCCS data is dominated by slower moving molecules that have an effective radius over seven times larger, according to the scaling proposed in the previous section. From this data we can conclude that the subset of Src_{16} anchors contributing to the FCCS curve are incorporated into slower-moving clusters, and that the large majority of Src_{16} anchors in the plasma membrane are freely diffusing as monomers.

Super resolution imaging of Src anchors

Based on the PIE-FCCS data presented above, we conclude that Src anchors are partially localized to slower moving clusters in the plasma membrane. These clusters are not visible in epifluorescence images, suggesting that they are smaller than the optical diffraction limit. To test this, we transfect Cos-7 cells with Src_{16} anchors fused to PS-CFP2, a photoactivatable fluorescent protein. By stochastically photoactivating a small subset of Src_{16}-PS-CFP2, we can localize their positions with 20 nm accuracy and build a spatial map of anchor positions. A representative live cell image is shown in Fig. 5A and 5B, where it is clear that there is clustering at several length scales. To quantify the size of the clusters we calculate a pair correlation function which has been used previously to quantify cluster size in PALM images.[25] Pair correlation functions

describe the probability of any given molecule having a neighbor at a distance r. The relatively low amplitude of the correlation function at short distances supports the conclusion that a minority of anchors are involved in clusters. The time decay of the correlation function decays to half its maximum at about 80 nm, and is similar across multiple cells. This observation is in agreement with a recent study using PALM to image a Src_{15} anchor in fixed Cos-7 cells.[17] In the report, the Src cluster size was not specified, but appears comparable to the reported ~70 nm clusters of the multiple acylated Lck anchor. Both the size and prevalence of clusters in the PALM images is consistent with the conclusion that Src_{16} anchors are weakly associated with membrane clusters in the range of 10-80 nm.

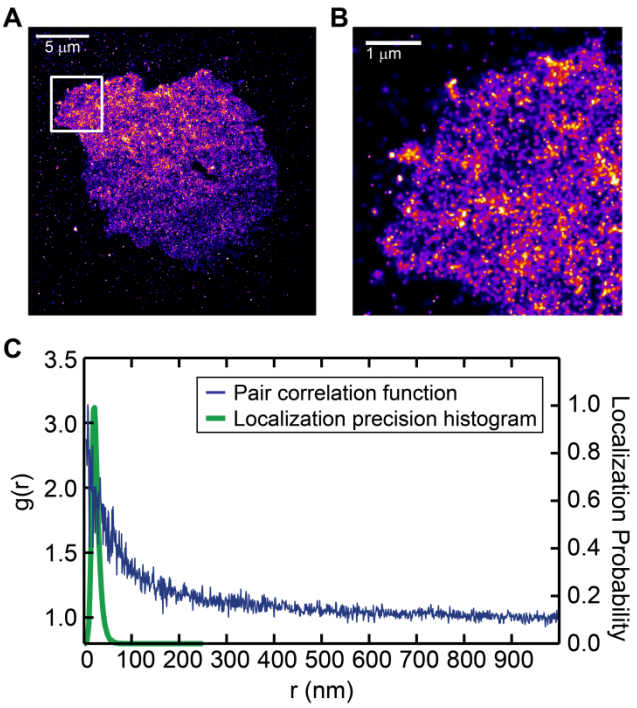

Figure 5 – PALM data of Src_{16} in a live cell show 10-80 nm clusters in the plasma membrane. Panel **(A)** is the PALM image constructed by reconvolving each localized molecule with a two-dimensional Gaussian function representing the localization precision. The white outlined area is magnified in panel **(B)**. Panel **(C)** shows the pair correlation function (blue) calculated as

described in the text for the cell pictured in (A). For comparison, the localization precision histogram is also plotted to show that the 80 nm decay is not due to the spatial resolution of the instrument.

The Src anchor is weakly clustered in Jurkat cells

We also looked at c-Src anchor in a different cell type to see whether or not the anchor clustering was unique to Cos-7 cells. PIE-FCCS measurements at room temperature of the anchor domain of the mouse isoform of c-Src ($mSrc_{16}$) in human leukemic Jurkat T cells showed the same trend as Src_{16} in Cos-7 cells at 20˚C with a density cross-over also near 500 molecules/μm^2. At low densities (<500 molecules/μm^2), average relative scaled correlation (scaled to *in vitro* samples of histidine-tagged fluorescent proteins on supported lipid bilayers and normalized to ~1.00) was 0.04 ± 0.18, while at high densities (>500 molecules/μm^2), the average scaled correlation went up to 0.24 ± 0.17.

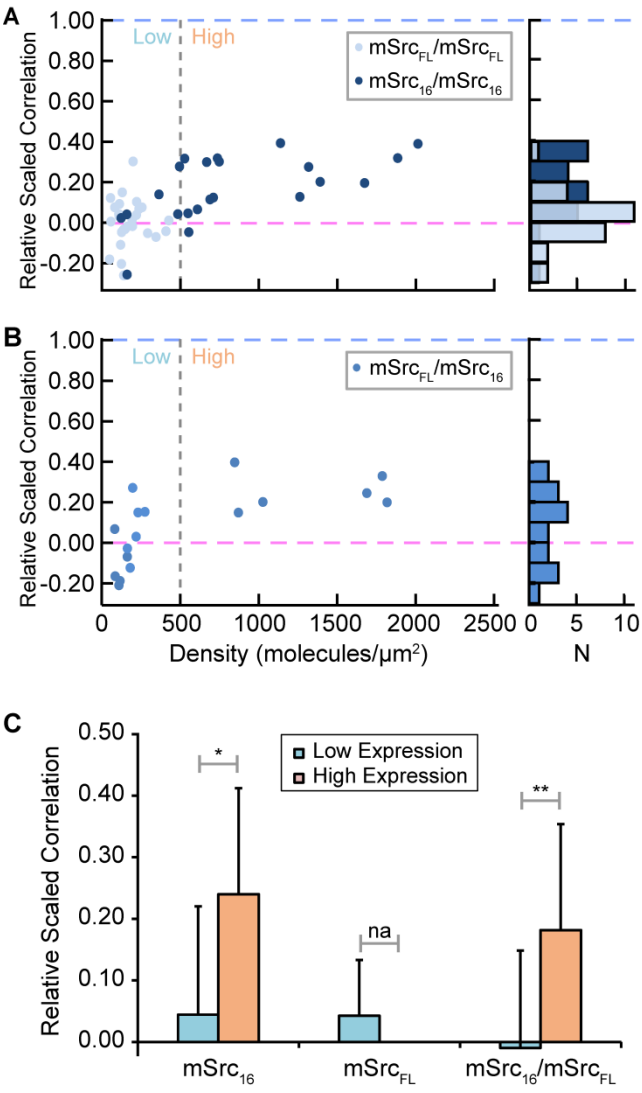

Figure 6 – The relative correlation of $mSrc_{16}$ and $mSrc_{FL}$ is density dependent in Jurkat cells at room temperature. **(A)** The scatter plot shows the relative scaled correlation for $mSrc_{16}$ (dark blue circles) and $mSrc_{FL}$ (light blue circles) with respect to membrane surface density. The graph on the right is a histogram (0.1 bin size) of the data in the left plot, which shares the same y-axis as the scatter plot. **(B)** The scatter plot shows the relative scaled correlation versus density for a hetero-expression of $mSrc_{16}$ and $mSrc_{FL}$. The graph on the right is a histogram of the data on the left as described for panel A. **(C)** Bar chart shows the average and standard deviation of the normalized relative correlation for the entire set of data for anchor alone, full length alone, and

anchor and full-length c-Src together and at two density ranges (low < 500 molecules/μm^2, high > 500 molecules/μm^2). (*p = 0.043, **p = 0.020)

Full length Src clusters with Src anchor

PIE-FCCS was also used to look at clustering of full-length mouse c-Src ($mSrc_{FL}$) in Jurkat cells, as well as the co-localization between the full length protein ($mSrc_{FL}$) and the lipid anchor ($mSrc_{16}$). The expression level of $mSrc_{FL}$ was consistently low, so there are no PIE-FCCS measurements of $mSrc_{FL}$ at high membrane densities (>500 molecules/μm^2). In $mSrc_{16}$/$mSrc_{FL}$ expressing cells, $mSrc_{16}$ generally outnumbered $mSrc_{FL}$ at high membrane densities, although only measurements with less than a 5:1 ratio of $mSrc_{16}$:$mSrc_{FL}$ were included in the data analysis (Fig. 6). The full length protein, $mSrc_{FL}$, did not exhibit any significant relative correlation (F_x = 0.04 ± 0.09) at low membrane densities. Cells expressing both $mSrc_{16}$ and $mSrc_{FL}$ showed low relative correlation at low densities (F_x = -0.01 ± 0.16), and increased relative correlation (F_x = 0.18 ± 0.17) at high membrane densities. From this data we conclude that both $mSrc_{16}$ and $mSrc_{FL}$ weakly partition into the same pre-existing membrane clusters observed in Cos-7 cells.

Comparing mobility of full-length Src and Src anchor

A comparison of the $mSrc_{16}$-eGFP and $mSrc_{FL}$-eGFP diffusion coefficients revealed that the anchor alone has only a slightly higher translational mobility than the full-length protein. On average, the effective diffusion coefficient, D_{eff}, of $mSrc_{16}$ across all densities was 1.36 ± 0.48 $\mu m^2 s^{-1}$ while D_{eff} of $mSrc_{FL}$ was 1.18 ± 0.56$\mu m^2 s^{-1}$ at 20 °C. Fig. 7A shows a summary of the data, including the mode of the distribution (red line), which happens to be slower than the average: $mSrc_{16}$ (1.07 $\mu m^2 s^{-1}$) and $mSrc_{FL}$ (0.89 $\mu m^2 s^{-1}$). From this we conclude that translational

mobility of Src is dominated by the lipid anchor and proximal amino acids, with only a minimal contribution from the cytosolic domain.

Rotational mobility of Src anchor is higher than full length Src

In addition to measuring the translational mobility of Src and the Src anchor, we also set out to measure its rotational mobility within the context of the plasma membrane. These experiments were carried out in Jurkat cells expressing either $mSrc_{16}$-eGFP or $mSrc_{FL}$-eGFP at 20 °C. Fluorescence anisotropy of $mSrc_{FL}$ and $mSrc_{16}$ both decayed at a much slower rate than the 2.7 ns fluorescence lifetime of GFP.[39] The $mSrc_{16}$ anisotropy decayed at a single-exponential rate with a rotational correlation time, θ = 52 ± 10 ns, and $mSrc_{FL}$ was much slower at θ = 110 ± 20 ns (Figure 7B and C). Both of these values are larger than the rotational correlation time of free GFP in solution of 10-20 ns.[40, 41] The slower rotational diffusion of $mSrc_{FL}$-eGFP indicates a higher prevalence of environmental interactions beyond those localized to the lipid anchor itself. This can be explained by simultaneous increases in protein gyration radius exposed to the viscosity of the cytosol, and additional interactions between the cytosolic domains of full-length Src and other membrane proteins. Based on the TRFA analysis, we conclude that the interactions of the cytosolic domain of Src with the local milieu of the cell membrane significantly decrease its rotational mobility.

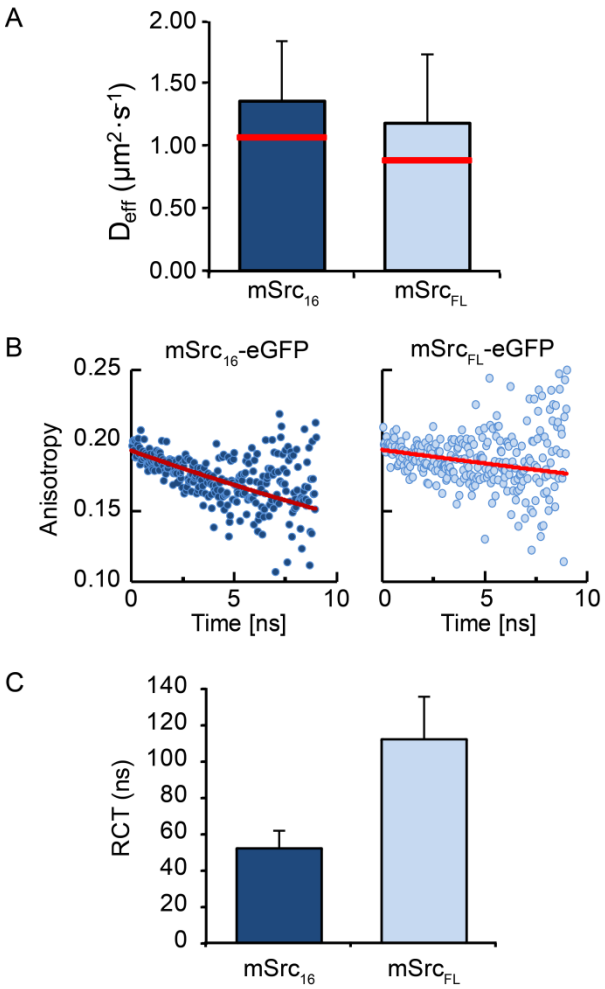

Figure 7 – Translational and rotational mobility of c-Src protein anchor versus full-length protein in Jurkat cells. **(A)** The FCS curves were fit to determine their characteristic decay times, τ_D, which is converted into a diffusion coefficient as described in Materials and Methods. Bar chart and error bars show the average and standard deviation of D_{eff} for $mSrc_{16}$-eGFP anchor (1.36 ± 0.48 $\mu m^2/s$) and $mSrc_{FL}$-eGFP full-length protein (1.18 ± 0.56 $\mu m^2/s$) in Jurkat cell plasma membrane at room temperature, while the red line marks the mode of the D_{eff} distribution for $mSrc_{16}$-eGFP (1.07 $\mu m^2/s$) and $mSrc_{FL}$-eGFP (0.89 $\mu m^2/s$). **(B)** Representative time resolved fluorescence anisotropy data of eGFP is shown for Src_{16} (left, dark blue circles) and Src_{FL} (right, light blue circles) with the corresponding single exponential fits in red. **(C)** Bar chart and error

bars show the average and standard deviation of the RCT for $mSrc_{16}$-eGFP (52 ± 10 ns) and $mSrc_{FL}$-eGFP (110 ± 20 ns) in Jurkat cell plasma membrane at 20 °C.

CONCLUSIONS

Lipidated protein organization has been the subject of numerous biophysical studies.[7-13] Rather than attempt to build a comprehensive model for this class of membrane anchored proteins, we instead focused on one important member of this class, the Src non-receptor tyrosine kinase. C-Src was the first member of the Src family kinases to be discovered and is a well-studied proto-oncogene. Despite its importance to cell signaling, the membrane organization of Src is not well-understood compared to other Src-family kinases. To isolate the organizational role of the membrane associated region of the protein, it has been common practice to express the anchor portion of the protein for biophysical studies. The earliest Src anchor constructs were composed of 14 or 16 N-terminal amino acids of the parent protein.[14, 42] In that early work, GFP-Src_{14} and GFP-Src_{16} were not found in the low-density, detergent resistant fractions of the cell membrane extract.[14, 42] Detergent resistant fractionation was an early assay for identifying lipid rafts, which are defined as small, dynamic membrane clusters enriched in cholesterol and sphingolipids.[43] This same observation was made later using a 15 amino acid sequence, GFP-Src_{15}, in cultured Jurkat T-cells.[15] Later, Sohn and Pierce also found that in B-Cells GFP-Src_{15} was detergent soluble, although a non-negligible portion was found in the detergent resistant fraction.[16] Finally in 2007, Rodgers observed that in Jurkat T-cells, there was an identifiable portion of Src_{15} (estimated to be 2%) in the detergent resistant fraction of the membrane extract.[7] Detergent extraction is a controversial method for studying membrane organization,[44] but the studies above were surprising because under the traditional raft hypothesis, saturated acyl chains, such as

myristate, should be found predominantly in the detergent resistant raft fraction.[45, 46] Indeed multiply acylated lipid-anchored proteins were found in raft fractionation.[7-11] This illustrates the need to characterize each anchor individually to determine its clustering behavior, including the size, mobility and likelihood of partitioning into clusters.

Attempts have also been made to measure the membrane organization of Src anchor chimeras with fluorescence imaging. Those studies focused on large (>1μm) clusters and could not reveal molecular-level clustering.[14, 15, 42] This is in part because the resolution of such methods was on the order of several hundred nanometers due to the optical diffraction limit, leaving them blind to molecular-scale interactions. Resonant energy transfer, or FRET, is sensitive to small intermolecular distances, and has been used to measure clustering of Src anchor chimeras. For example, Src_{15} was co-expressed as a FRET pair with CFP and YFP in Jurkat T-Cells, and some FRET was observed.[7] However, the data in that study were poorly correlated with acceptor intensity, which made it difficult to quantify the level of FRET arising from specific, long-lived interactions. Furthermore, such FRET assays cannot resolve the size of the membrane clusters and are insensitive to FRET pairs occupying the same cluster but separated well beyond the Förster radius. FRET also cannot resolve the mobility of Src anchors or of the larger clusters with which they have been hypothesized to associate.

There is one report of newly developed super-resolution fluorescence microscopy methods being applied to Src clustering.[17] Photoactivated localization microscopy (PALM) was used to image a Src_{15} anchor chimera in fixed cells with sub-diffraction limit precision. In this report, the Src cluster size was not specified, but appeared comparable to the reported ~70 nm clusters of the multiple acylated Lck anchor. While super-resolution methods like PALM have

the ability to observe cluster size and density, they cannot directly measure the dynamics of the clusters, especially within fixed-cell membranes.

Using a combination of fluorescence spectroscopy and microscope methods, we have measured the clustering of Src_{16} in Cos-7 and Jurkat T-Cells. Our results show that the cSrc-derived membrane anchor transiently associates with a pre-existing network of plasma membrane clusters. The high mobility of Src allows it to play a role in, for example, cell migration at the leading edge of lamellapodia, while its association with large clusters allows it to integrate with protein clusters associated with mature focal adhesions.[6, 47] The experimental approach taken in this work demonstrates that a combination of advanced tools in fluorescence spectroscopy and imaging can reveal the heterogeneous behavior of membrane proteins in a live cell environment. We expect this approach to yield substantial insight to membrane receptor signaling, where protein complex formation during cell signaling events is still not well understood.

AKNOWLEDGEMENTS

This work was supported by the Director, Office of Science, Office of Basic Energy Sciences, Chemical Sciences, Geosciences and Biosciences Division of the U.S. Department of Energy under Contract No. DE-AC02_05CH11231.

REFERENCES

1. Casey, P. J. Protein Lipidation in Cell Signaling. *Science* **1995,** *268*, 221-225.

2. Resh, M. D. Trafficking and Signaling by Fatty-Acylated and Prenylated Proteins. *Nat Chem Biol* **2006,** *2*, 584-590.

3. Resh, M. D. Fatty Acylation of Proteins: New Insights into Membrane Targeting of Myristoylated and Palmitoylated Proteins. *Biochimica et Biophysica Acta (BBA) - Molecular Cell Research* **1999,** *1451*, 1-16.

4. Wright, M.; Heal, W.; Mann, D.; Tate, E. Protein Myristoylation in Health and Disease. *Journal of Chemical Biology* **2010,** *3*, 19-35.

5. Murray, D.; Ben-Tal, N.; Honig, B.; McLaughlin, S. Electrostatic Interaction of Myristoylated Proteins with Membranes: Simple Physics, Complicated Biology. *Structure* **1997,** *5*, 985-989.

6. Seong, J.; Lu, S.; Ouyang, M.; Huang, H.; Zhang, J.; Frame, M. C.; Wang, Y. Visualization of Src Activity at Different Compartments of the Plasma Membrane by Fret Imaging. *Chemistry & Biology* **2009,** *16*, 48-57.

7. Chichili, G. R.; Rodgers, W. Clustering of Membrane Raft Proteins by the Actin Cytoskeleton. *J. Biol. Chem.* **2007,** *282*, 36682-36691.

8. Zacharias, D. A.; Violin, J. D.; Newton, A. C.; Tsien, R. Y. Partitioning of Lipid-Modified Monomeric Gfps into Membrane Microdomains of Live Cells. *Science* **2002,** *296*, 913-916.

9. Lommerse, P. H. M.; Vastenhoud, K.; Pirinen, N. J.; Magee, A. I.; Spaink, H. P.; Schmidt, T. Single-Molecule Diffusion Reveals Similar Mobility for the Lck, H-Ras, and K-Ras Membrane Anchors. *Biophys. J.* **2006,** *91*, 1090-1097.

10. Abankwa, D.; Vogel, H. A Fret Map of Membrane Anchors Suggests Distinct Microdomains of Heterotrimeric G Proteins. *J. Cell Sci.* **2007,** *120*, 2953-2962.

11. Triffo, S. B.; Huang, H. H.; Smith, A. W.; Chou, E. T.; Groves, J. T. Monitoring Lipid Anchor Organization in Cell Membranes by Pie-Fccs. *J. Am. Chem. Soc.* **2012,** *134*, 10833-10842.

12. Goodwin, J. S.; Drake, K. R.; Remmert, C. L.; Kenworthy, A. K. Ras Diffusion Is Sensitive to Plasma Membrane Viscosity. *Biophys. J.* **2005,** *89*, 1398-1410.

13. Sharma, P.; Varma, R.; Sarasij, R. C.; Ira; Gousset, K.; Krishnamoorthy, G.; Rao, M.; Mayor, S. Nanoscale Organization of Multiple Gpi-Anchored Proteins in Living Cell Membranes. *Cell* **2004,** *116*, 577-589.

14. McCabe, J. B.; Berthiaume, L. G. N-Terminal Protein Acylation Confers Localization to Cholesterol, Sphingolipid-Enriched Membranes but Not to Lipid Rafts/Caveolae. *Mol. Biol. Cell* **2001,** *12*, 3601-3617.

15. Rodgers, W. Making Membranes Green: Construction and Characterization of Gfp-Fusion Proteins Targeted to Discrete Plasma Membrane Domains. *Biotechniques* **2002,** *32*, 1044-+.

16. Sohn, H. W.; Tolar, P.; Jin, T.; Pierce, S. K. Fluorescence Resonance Energy Transfer in Living Cells Reveals Dynamic Membrane Changes in the Initiation of B Cell Signaling. *Proc. Natl. Acad. Sci. U.S.A.* **2006,** *103*, 8143-8148.

17. Owen, D. M.; Rentero, C.; Rossy, J.; Magenau, A.; Williamson, D.; Rodriguez, M.; Gaus, K. Palm Imaging and Cluster Analysis of Protein Heterogeneity at the Cell Surface. *Journal of Biophotonics* **2010,** *3*, 446-454.

18. Dragsten, P.; Henkart, P.; Blumenthal, R.; Weinstein, J.; Schlessinger, J. Lateral Diffusion of Surface Immunoglobulin, Thy-1 Antigen, and a Lipid Probe in Lymphocyte Plasma Membranes. *Proc. Natl. Acad. Sci. U.S.A.* **1979,** *76*, 5163-5167.

19. Lee, G. M.; Ishihara, A.; Jacobson, K. A. Direct Observation of Brownian Motion of Lipids in a Membrane. *Proc. Natl. Acad. Sci. U.S.A.* **1991,** *88*, 6274-6278.

20. Schwille, P.; Korlach, J.; Webb, W. W. Fluorescence Correlation Spectroscopy with Single-Molecule Sensitivity on Cell and Model Membranes. *Cytometry* **1999,** *36*, 176-182.

21. Endres, Nicholas F.; Das, R.; Smith, Adam W.; Arkhipov, A.; Kovacs, E.; Huang, Y.; Pelton, Jeffrey G.; Shan, Y.; Shaw, David E.; Wemmer, David E., et al. Conformational Coupling across the Plasma Membrane in Activation of the Egf Receptor. *Cell* **2013,** *152*, 543-556.

22. Smith, A. W.; Smoligovets, A. A.; Groves, J. T. Patterned Two-Photon Photoactivation Illuminates Spatial Reorganization in Live Cells. *J. Phys. Chem. A* **2011,** *115*, 3867-3875.

23. Gould, T. J.; Verkhusha, V. V.; Hess, S. T. Imaging Biological Structures with Fluorescence Photoactivation Localization Microscopy. *Nat. Protocols* **2009,** *4*, 291-308.

24. Hess, S. T.; Gould, T. J.; Gudheti, M. V.; Maas, S. A.; Mills, K. D.; Zimmerberg, J. Dynamic Clustered Distribution of Hemagglutinin Resolved at 40 Nm in Living Cell Membranes Discriminates between Raft Theories. *Proc. Natl. Acad. Sci. U.S.A.* **2007,** *104*, 17370-17375.

25. Baksh, M. M.; Jaros, M.; Groves, J. T. Detection of Molecular Interactions at Membrane Surfaces through Colloid Phase Transitions. *Nature* **2004,** *427*, 139-141.

26. Jura, N.; Endres, N. F.; Engel, K.; Deindl, S.; Das, R.; Lamers, M. H.; Wemmer, D. E.; Zhang, X.; Kuriyan, J. Mechanism for Activation of the Egf Receptor Catalytic Domain by the Juxtamembrane Segment. *Cell* **2009,** *137*, 1293-1307.

27. Foo, Yong H.; Naredi-Rainer, N.; Lamb, Don C.; Ahmed, S.; Wohland, T. Factors Affecting the Quantification of Biomolecular Interactions By fluorescence Cross-Correlation Spectroscopy. *Biophys. J.* **2012,** *102*, 1174-1183.

28. Golebiewska, U.; Nyako, M.; Woturski, W.; Zaitseva, I.; McLaughlin, S. Diffusion Coefficient of Fluorescent Phosphatidylinositol 4,5-Bisphosphate in the Plasma Membrane of Cells. *Mol. Biol. Cell* **2008,** *19*, 1663-1669.

29. Kuhn, T.; Ihalainen, T. O.; Hyvaluoma, J.; Dross, N.; Willman, S. F.; Langowski, J.; Vihinen-Ranta, M.; Timonen, J. Protein Diffusion in Mammalian Cell Cytoplasm. *PLoS ONE* **2011,** *6*, e22962.

30. Mullineaux, C. W.; Nenninger, A.; Ray, N.; Robinson, C. Diffusion of Green Fluorescent Protein in Three Cell Environments in Escherichia Coli. *J. Bacteriol.* **2006,** *188*, 3442-3448.

31. Digman, M. A.; Brown, C. M.; Sengupta, P.; Wiseman, P. W.; Horwitz, A. R.; Gratton, E. Measuring Fast Dynamics in Solutions and Cells with a Laser Scanning Microscope. *Biophys. J.* **2005,** *89*, 1317-1327.

32. Kang, M.; Day, C. A.; Kenworthy, A. K.; DiBenedetto, E. Simplified Equation to Extract Diffusion Coefficients from Confocal Frap Data. *Traffic* **2012,** *13*, 1589-1600.

33. Saffman, P. G.; Delbruck, M. Brownian Motion in Biological Membranes. *Proc. Natl. Acad. Sci. U.S.A.* **1975,** *72*, 3111-3113.

34. Naji, A.; Levine, A. J.; Pincus, P. A. Corrections to the Saffman-Delbruck Mobility for Membrane Bound Proteins. *Biophys. J.* **2007,** *93*, L49-L51.

35. Chung, I.; Akita, R.; Vandlen, R.; Toomre, D.; Schlessinger, J.; Mellman, I. Spatial Control of Egf Receptor Activation by Reversible Dimerization on Living Cells. *Nature* **2010,** *464*, 783-787.

36. Heinemann, F.; Vogel, Sven K.; Schwille, P. Lateral Membrane Diffusion Modulated by a Minimal Actin Cortex. *Biophys. J.* **2013,** *104*, 1465-1475.

37. Zhao, J.; Wu, J.; Veatch, Sarah L. Adhesion Stabilizes Robust Lipid Heterogeneity in Supercritical Membranes at Physiological Temperature. *Biophys. J.* **2013,** *104*, 825-834.

38. Machta, Benjamin B.; Papanikolaou, S.; Sethna, James P.; Veatch, Sarah L. Minimal Model of Plasma Membrane Heterogeneity Requires Coupling Cortical Actin to Criticality. *Biophys. J.* **2011,** *100*, 1668-1677.

39. Suhling, K.; Siegel, J.; Phillips, D.; French, P. M. W.; Leveque-Fort, S.; Webb, S. E. D.; Davis, D. M. Imaging the Environment of Green Fluorescent Protein. *Biophys. J.* **2002,** *83*, 3589-3595.

40. Hink, M. A.; Griep, R. A.; Borst, J. W.; van Hoek, A.; Eppink, M. H. M.; Schots, A.; Visser, A. J. W. G. Structural Dynamics of Green Fluorescent Protein Alone and Fused with a Single Chain Fv Protein. *J. Biol. Chem.* **2000,** *275*, 17556-17560.

41. Swaminathan, R.; Hoang, C. P.; Verkman, A. S. Photobleaching Recovery and Anisotropy Decay of Green Fluorescent Protein Gfp-S65t in Solution and Cells: Cytoplasmic Viscosity Probed by Green Fluorescent Protein Translational and Rotational Diffusion. *Biophys. J.* **1997,** *72*, 1900-1907.

42. McCabe, J. B.; Berthiaume, L. G. Functional Roles for Fatty Acylated Amino-Terminal Domains in Subcellular Localization. *Mol. Biol. Cell* **1999,** *10*, 3771-3786.

43. Pike, L. J. Rafts Defined: A Report on the Keystone Symposium on Lipid Rafts and Cell Function. *J. Lipid Res.* **2006,** *47*, 1597-1598.

44. Lingwood, D.; Simons, K. Lipid Rafts as a Membrane-Organizing Principle. *Science* **2010,** *327*, 46-50.

45. Pike, L. J. The Challenge of Lipid Rafts. *J. Lipid Res.* **2009,** *50*, S323-328.

46. Levental, I.; Grzybek, M.; Simons, K. Greasing Their Way: Lipid Modifications Determine Protein Association with Membrane Rafts. *Biochemistry* **2010,** *49*, 6305-6316.

47. de Diesbach, P.; Medts, T.; Carpentier, S.; D'Auria, L.; Van Der Smissen, P.; Platek, A.; Mettlen, M.; Caplanusi, A.; van den Hove, M.-F.; Tyteca, D., et al. Differential Subcellular Membrane Recruitment of Src May Specify Its Downstream Signalling. *Exp. Cell Res.* **2008,** *314*, 1465-1479.

TOC GRAPHIC

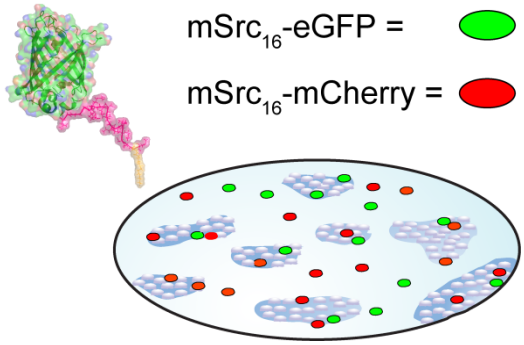

DISCLAIMER